
Optimizing Memory Placement using Evolutionary Graph Reinforcement Learning

Shauharda Khadka *
Intel Labs

Estelle Aflalo *
Intel Israel

Mattias Marder *
Intel Israel

Avrech Ben-David *
Technion

Santiago Miret
Intel Labs

Hanlin Tang
Intel Labs

Shie Mannor
Technion

Tamir Hazan
Technion

Somdeb Majumdar †
Intel Labs

Abstract

As modern neural networks have grown to billions of parameters, meeting tight latency budgets has become increasingly challenging. Approaches like compression, sparsification and network pruning have proven effective to tackle this problem - but they rely on modifications of the underlying network. In this paper, we look at a complimentary approach of optimizing how tensors are mapped to on-chip memory in an inference accelerator while leaving the network parameters untouched. Since different memory components trade off capacity for bandwidth differently, a sub-optimal mapping can result in high latency. We introduce evolutionary graph reinforcement learning (EGRL) - a method combining graph neural networks, reinforcement learning (RL) and evolutionary search - that aims to find the optimal mapping to minimize latency. Furthermore, a set of fast, stateless policies guide the evolutionary search to improve sample-efficiency. We train and validate our approach directly on the Intel NNP-I chip for inference using a batch size of 1. EGRL outperforms policy-gradient, evolutionary search and dynamic programming baselines on BERT, ResNet-101 and ResNet-50. We achieve 28-78% speed-up compared to the native NNP-I compiler on all three workloads.

1 Introduction

The proliferation of deep learning (DL) has been fueled, in part, by a rapid growth in the size and complexity of deep neural network (DNN) [Dean et al., 2012, Ying et al., 2018]. This has spurred the rapid development of hardware [Wang et al., 2016, Jouppi et al., 2017] and software [Abadi et al., 2016, Paszke et al., 2018, Cyphers et al., 2018] dedicated to deep learning workloads that seek to optimize critical performance metrics like throughput and power efficiency [Mattson et al., 2020]. Compiler optimizations to map the tensors of a neural network’s computational graph to the memory units on host hardware is a critical challenge. Since different memory types trade off bandwidth and capacity differently, a sub-optimal mapping could significantly increase latency.

For DL inference, the computational graph is static and placement can be pre-planned instead of relying on online cache management [Zhang et al., 2020, Shi et al., 2019]. However, this is especially challenging with DNNs due to the high dimensional search space. For example, ResNet-50 [He et al., 2016a] has 57 operational layers; mapping each activation and weight tensor to three (DRAM, LLC, and SRAM) memory caches represents $3^{(2*57)} \approx 10^{54}$ possible decisions. Since optimizing this mapping is intractable with traditional approaches such as dynamic programming [Bellman, 1954], current solutions primarily rely on manually-tuned heuristic rules encoded in a compiler.

*Equal Contribution

†Correspondence to: <somdeb.majumdar@intel.com>

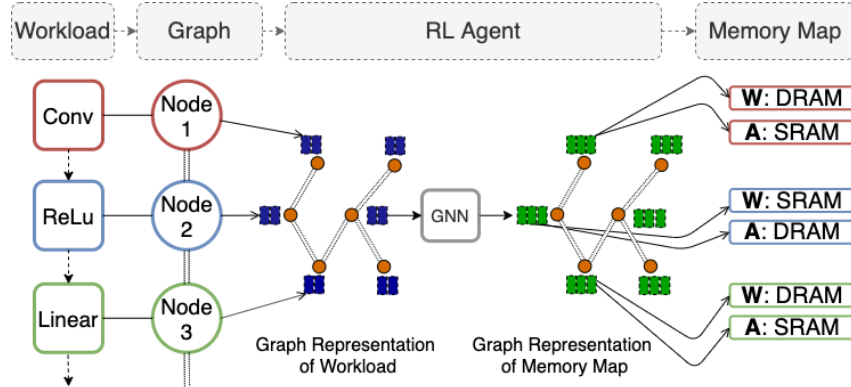


Figure 1: Workflow of Graph RL agent mapping weights (W) and activations (A) to various memories (e.g. DRAM, SRAM).

In this paper, we investigate if a machine learning based solution could address this problem in a scalable manner. We formulate the task as a Reinforcement Learning (RL) problem, where an agent performs actions to map each layer’s weights and activations to one of several memory caches on the chip (e.g. DRAM, LLC and SRAM).

In addition to the extremely large action space, the reward is end-to-end latency, which is a sparse and noisy learning signal, which we demonstrate is unsuitable for purely gradient-based Deep RL algorithms. Instead, we contribute Evolutionary Graph RL (EGRL), an extension of CERL [Khadka et al., 2019], a population based method which previously performed well in sparse-reward tasks by combining fast policy gradient (PG) learning with a stable evolutionary algorithm (EA). Since the action spaces explored in this paper are several orders of magnitude larger than the ones explored in CERL, we also needed a mechanism to improve the sample-efficiency of the slow EA component. Thus we introduce Boltzmann chromosomes - a set of fast, stateless policies that accelerate evolution by providing partially optimized solutions as anchors.

Further, we employ a graph neural network (GNN) [Wu et al., 2020, Scarselli et al., 2008] to represent our policy. This allows our agent to natively process computational graphs representing deep learning workloads, enabling generalization over workloads of arbitrary size and connectivity. Figure 1 illustrates the high level overview of our method.

We demonstrate our solution on the Intel Neural Network Processor for Inference (NNP-I) [Wechsler et al., 2019], a deep learning accelerator with constraints on memory capacity, bandwidth and power. This is a key differentiator from prior works such as REGAL [Paliwal et al., 2020] that assume infinite bandwidth and memory that are not practical on real hardware. Additionally, we consider single-batch inference. While large batch sizes have greater computational efficiency (e.g., [Boudoukh et al., 2020] on NNP-I), they are sub-optimal for a given inference example due to the latency associated with queuing up a batch. Therefore, single-batch inference is key to many time-critical applications [Park et al., 2018] where an individual inference query needs to be processed in real-time.

Results on ResNet-50 [He et al., 2016b], ResNet-101 [He et al., 2016a] and BERT [Devlin et al., 2018], show that EGRL significantly outperforms the chipset’s native compiler across all workloads, and exceeds the performance of a dynamic programming approach and a policy-gradient approach.

Specifically, the contributions of this work are:

1. A generalized GNN-based policy representation that can natively process deep learning workloads without the need for serialized, layer-dependent representations.
2. EGRL, a scalable population-based algorithm that can effectively train on sparse and noisy feedback from the host hardware.
3. An RL agent that trains directly on the hardware, with a feedback mechanism for constraint violation. Thus, we are able to directly deploy and test on hardware.

2 Background and Related Work

We consider a Markov Decision Process (MDP) setting defined by the tuple $\{\mathcal{S}, \mathcal{A}, P, r\}$, with a state space \mathcal{S} , a discrete action space \mathcal{A} , an unknown state transition probability P that maps a state s_t at time t and an action a_t to the probability of a next state s_{t+1} , and a reward r_t provided by the environment for a given state transition. We learn a policy π that maximizes the expectation of the total episodic return from time-step t , $R_t = \sum_{k=0}^{\infty} \gamma^k r_{t+k}$, where $\gamma \in [0, 1]$ is the discount factor. Policy Gradient (PG) methods re-frame this goal of maximizing the expected return as the minimization of a loss function $L(\theta)$ where θ encapsulates the agent parameters. A widely used method is Soft-Actor Critic (SAC) [Haarnoja et al., 2018], a model-free algorithm developed for continuous high-dimensional settings. SAC uses an actor-critic architecture with separate networks for the policy and the Q-value function. A stochastic Gaussian policy enables it to use a maximum entropy objective [Ziebart et al., 2008] through which it demonstrates state-of-the-art results.

Collaborative Evolutionary Reinforcement Learning (CERL) [Khadka and Tumer, 2018, Khadka et al., 2019] combines Evolutionary Algorithms (EAs) [Floreano et al., 2008, Lüders et al., 2017, Fogel, 2006, Spears et al., 1993] with PG. It diversifies exploration by allowing a population of EA policies to add data to a central replay buffer shared by a population of PG learners. Since the gradient-free EA directly optimizes for episode-wide return, it biases exploration, and implicitly the PG policies, towards states with higher long-term returns. Concurrently, PG policies are inserted into the EA population in order to provide better search anchors for EA. CERL’s integrated framework was shown to outperform its components (PG and EA) in isolation. We directly build on CERL because the memory mapping solution inherently relies on optimizing a very sparse feedback signal (e.g., latency) that is obtained at the end of an inference run through a workload.

Graph Neural Networks (GNNs) were first proposed as a recursive message passing framework with learnable parameters [Gori et al., 2005]. Subsequent work relaxed the architecture to work as a generalization of convolutional networks resulting in a broader graph data structure [Xu et al., 2015, Sukhbaatar et al., 2016]. Pertinently, GNNs have been paired with RL for tackling fundamental combinatorial optimization problems such as Minimum Vertex Cover, Maximum Cut and the Traveling Salesman Problem. [Dai et al., 2018, Mittal et al., 2019].

Optimizing Hardware using Machine Learning: Deep RL was used in [Mirhoseini et al., 2020] to learn subsystems placement to optimize power, performance and space. Similarly, AutoTVM [Chen et al., 2018] employed learning to optimize low-level implementations of operators in tensor programs. On the same note, Placeto [Addanki et al., 2018] combines GNNs and RL to achieve effective device placements in distributed clusters.

A closely related work is REGAL [Paliwal et al., 2020] which optimizes run-time and peak-memory via hardware placement. It utilizes a graph representation with a genetic algorithm (GA) guided by RL. The RL agent predicts the parameters of GA - a form of indirect information transfer - while GA directly optimizes the final strategy. In contrast, our RL and EA components each co-optimize the mapping strategies via direct information transfer (policy migration) and a shared replay buffer. REGAL’s assumes infinite bandwidth and memory, whereas we train and validate entirely on physical hardware introducing specific mechanisms to incentivize compiler-valid mappings. This ensures that our solutions are performant under real-world operating conditions and closer to production-use.

3 Method

We formulate the hardware mapping problem as an MDP and use RL to train a solution. Figure 1 illustrates the high-level formulation of our workflow.

3.1 MDP Formulation

State: A major challenge in memory mapping is to find effective general representations for large and complex workloads. One approach is to convert the computational graph into sequential segments [He et al., 2018, Wang et al., 2019] that are fed to the RL policy one-by-one. A reward can then be computed at the end of each episode. While this sequential approach is simple, it struggles to generalize to workloads with varying depths and complexity. Furthermore, the serial nature of this approach limits the speed of learning that can be obtained by parallelization.

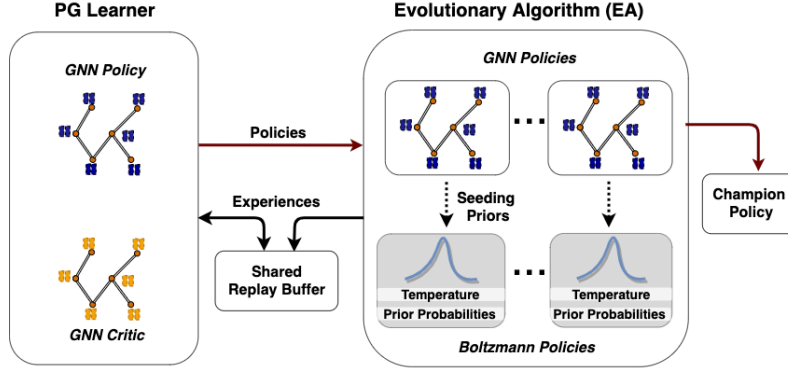


Figure 2: EGRL Architecture: EA and PG operate concurrently via a shared replay buffer. EA comprises sub-populations of GNN and Boltzmann policies. PG policy periodically migrates to EA.

To address these limitations, we encapsulate the workload as a directed graph \mathcal{G} , whose nodes represent operational layers (e.g. convolution, pooling, etc.), and edges indicate the connectivity between layers. Each node’s features describe its operation as well as characteristics of the weights and activation tensors associated with it (e.g. byte-size of the weights, kernel size, etc.). A detailed description of the node features can be found in Appendix A. Since all the outgoing edges of a node denote the same output tensor, their associated information are encapsulated in their source node features, leaving the edges featureless.

Action: Given the graph representation of the DL workload, \mathcal{G} , we use a GNN policy π to map it to a set of memory mapping decisions \mathcal{M}_π . Algorithm 1 details this process. The goal of π is to maximize the improvement in a performance metric Ω . The agent takes two distinct sub-actions per node, each choosing between one of three memory units (DRAM, LLC and SRAM): one for weights and the other for the activations (Line 5). The agent’s complete memory map \mathcal{M}_π is sent to the compiler. If any of the mapping decisions cannot be executed on the hardware (i.e., invalid mapping), the compiler rectifies them and outputs a modified map, \mathcal{M}_C , that is fully executable (Line 6).

Reward: In a standard RL setting, one can generally constrain the action space to avoid invalid actions. However, in our problem setting, constraining the action explicitly requires reproducing the compiler’s logic for valid mappings, which would vary across hardware and compiler versions. In order to keep the RL algorithm independent of the compiler logic, we formulate separate reward domains for invalid and valid mappings. If the agent produces any invalid mapping that the compiler re-assigns, we do not execute an inference. Instead, we formulate a negative reward as a function of the re-assigned bytes ratio, to quantify the extent of the invalidity (Line 12 in Algorithm 1). This formulation allows us to avoid implementing the compiler logic explicitly - instead relying on a negative feedback that enables the agent to implicitly learn the rules for valid mappings.

When the agent does produce a fully valid mapping, we execute inference and compute a positive reward. This reward is a function of the agent performance score normalized by that of the native compiler (Line 10 in Algorithm 1). While the normalization is not necessary when training on a single workload, it allows for flexibility to concurrently train on multiple workloads that might have a wide range of scores. For our application, we maximize the reciprocal of latency.

Algorithm 1 Agent’s Interaction with the Environment

- 1: **Initialize** workload f , policy π , perf. metric Ω
 - 2: **Initialize** compiler \mathcal{C} and graph transform \mathcal{G}
 - 3: $\mathcal{G}(f) \leftarrow f$ ▷ Workload to graph
 - 4: **for** each iteration i **do**
 - 5: $\mathcal{M}_\pi = \pi_i(\mathcal{G})$ ▷ Agent’s map
 - 6: $\mathcal{M}_C = \mathcal{C}(\mathcal{M}_\pi)$ ▷ Compile agent’s map
 - 7: $\epsilon_{\mathcal{M}} = \mathcal{M}_\pi \parallel \mathcal{M}_C$ ▷ Mapping error
 - 8: **if** $\epsilon_{\mathcal{M}} == 0$ **then**
 - 9: $\Omega = \mathcal{I}(\mathcal{M}_C)$ ▷ Run inference
 - 10: $r_{\mathcal{M}} = \left(\frac{\Omega}{\Omega_{baseline}}\right)^2$ ▷ Positive reward
 - 11: **else**
 - 12: $r_{\mathcal{M}} = -\epsilon_{\mathcal{M}}$ ▷ Negative reward
 - 13: **end if**
 - 14: $\pi_{i+1} \leftarrow \pi_i$ ▷ Update policy
 - 15: **end for**
-

3.2 Training

Our training algorithm, EGRL, builds on the CERL framework [Khadka et al., 2019] to tackle variable-sized, multi-discrete action settings. Figure 2 illustrates the high level architecture of EGRL. It comprises of a single PG learner (a GNN) and an EA population containing a mixture of GNN and Boltzmann policies, as detailed below. A round of rollouts is conducted to compute the fitness for each individual in the population. All data generated across the population is stored in the PG learner’s replay buffer. The population then goes through probabilistic selection, mutation and crossover operators commensurate with the fitnesses computed.

Concurrently, the PG learner updates its actor and critic by sampling from the shared replay buffer. It periodically migrates to the EA population as a form of information transfer. At any given time, the top-ranked policy in the EA population is chosen for deployment. A detailed description can be found in the Appendix while a truncated codebase can be found in ³ for reference.

GNN Policy: Given the large state space representing the operational layers of each workload, it was critical to develop a policy representation that could exploit the inherent dependencies between them. We implemented a Graph U-Net policy based on [Gao and Ji, 2019]. The Graph U-Net leverages bidirectional graph convolutions and graph attention operations to derive invariant intermediate node features. This representation afforded us a multidimensional action-space where the agent can simultaneously affect the memory mappings for all weights and activations of the workload. This enables our agent to generalize across workloads of varying sizes and diversity of operations.

Boltzmann Chromosome: Figure 3 illustrates the Boltzmann chromosome, an additional policy representation we introduced into the population based on the Boltzmann softmax operation [Asadi and Littman, 2017]. Each Boltzmann chromosome is parameterized by a set of prior probabilities (P) and a temperature (T) for each node. To compute an action for each node, we sample from the Boltzmann softmax function using that node’s P and T . In contrast to a GNN policy, which is parameterized by its weights and produces mappings following a feed-forward operation, the Boltzmann chromosome directly represents the mapping decision and its associated uncertainty. Thus it is significantly faster to compute and is an ideal embedding for search-based EA method. The ratio of exploration

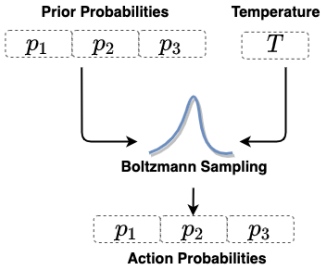


Figure 3: Boltzmann Chromosome

to exploitation is controlled by the temperature T parameter directly. A lower temperature favors decisions close to the prior P while a higher temperature encourages exploration further from P . Crucially, T is learned (via evolution) for each node independently which allows for varying degrees of exploration-exploitation across different mapping decisions simultaneously.

Mixed Population: The EA population concurrently holds both GNN and Boltzmann policies. Crucially, all policies share data and benefit from the joint exploration. The PG based GNN policy can directly leverage the states explored by the Boltzmann policy to compute gradients. Conversely, as shown in Figure 2, the Boltzmann policy’s prior P is periodically seeded using the GNN policy’s posterior probability distribution - thus enabling it to directly bootstrap from the GNN population.

Policy Gradient Algorithm: We build on SAC [Haarnoja et al., 2018], making modifications to tackle our large multi-discrete actions space. Please refer to Appendix D for a detailed description.

4 Experiments

Domain: We evaluated the performance of our agents on the Intel NNP-I hardware. For a given DNN workload, our agents controlled how their intermediate tensors are mapped to memory units on the chip. We then report the resulting latency as measured directly in the hardware. We conduct both training and testing entirely on the physical hardware.

Workloads Tested: We benchmarked on three popular workloads. ResNet-50 [He et al., 2016a], with 57 nodes, is widely used for benchmarks such as MLPerf [Reddi et al., 2019]. ResNet-101, with 108 nodes, allowed us to test for scale. Lastly, BERT [Devlin et al., 2018], with 376 nodes, is a state-of-the-art natural language processing model. This allowed us to test for scale and generalization

³ <https://anonymous.4open.science/r/290d6d70-5324-4d13-8458-19de1dc6aeed>

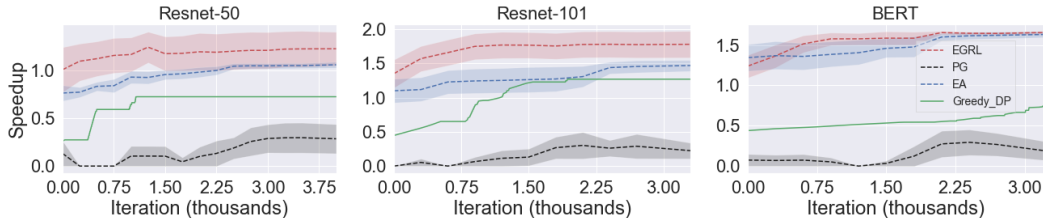


Figure 4: Speedup for different workloads, normalized to the heuristic compiler performance. EGRL consistently outperforms all baselines. Error bars indicate standard deviation over $n = 5$ runs.

of our approach. Since the action space for a workload with N nodes is $3^{(2N)}$, the corresponding sizes of the action spaces are $3^{114} \approx 10^{54}$, $3^{216} \approx 10^{103}$ and $3^{752} \approx 10^{358}$ respectively.

Metrics Reported: We define *speedup* as the relative improvement in latency achieved by the agent’s mapping versus that of the compiler. A score greater than 1 indicates an improvement in latency while a score between 0 and 1 indicates a degradation. A score of 0 indicates an invalid mapping. We conduct 5 independent statistical runs and report the mean and standard deviation. Further, we report all speedups against iterations where an iteration refers to an inference process in the physical hardware. To ensure a fair comparison between population-based and single-policy methods, we count the iterations cumulatively across the population.

Baseline: We use the Intel NNP-I’s default compiler as our baseline. The compiler consists of a collection of heuristic rules specific to the memory and compute capacity of the hardware and the nature of the specific workload. We also implement a number of learning and search based agents for comparison, detailed below:

Greedy Dynamic Programming (DP) agent, inspired by DP methods for optimization [Andonov et al., 2000, Bertsimas and Thiele, 2004], makes layer-wise greedy decisions directly on the workload. Since we have 3 memory choices for 2 types of tensors, we have 9 distinct decisions per node. The Greedy-DP agent tries all possible maps for the first node (keeping all other mapping static), and chooses the action that leads to the maximum reward. It repeats this for every single node in the workload. Once it reaches the end, it circles back to the first node and repeats the entire process conducting several passes. The Greedy-DP essentially assumes conditional independence of mapping across the layers to reduce the solution space from $9^N \rightarrow 9 * N$, where N is the number of layers. While the conditional independence is a fairly naïve assumption, running multiple passes through the graph produces a reasonable solution.

Evolutionary Algorithm (EA) agent ablates the policy gradient component within EGRL and uses only the evolutionary component to train the RL agent.

Policy Gradient (PG) agent ablates the evolutionary component of EGRL and tests the modified SAC-discrete algorithm in isolation.

5 Results

Figure 4 shows the relative speedup achieved for the various agents tested on the ResNet-50, ResNet-101 and BERT workloads. The speedups are reported relative to the compiler and are measured directly on the NNP-I hardware. Results demonstrate that EA and EGRL significantly improve upon the compiler consistently across all three workloads. Greedy-DP approaches baseline performance while the PG agent fails to reach it.

ResNet-50: EGRL and EA significantly outperform the baseline compiler as well as the other agents reaching a final speedup of 1.28 and 1.06, respectively. Greedy-DP underperforms the compiler at 0.72 while PG converges to 0.29.

ResNet-101: EGRL significantly outperform the baseline compiler and all other agents reaching a final speedup of 1.78. EA comes second, converging to a final speedup of 1.47. This performance gap demonstrates the role played by the collaborative learning using the shared replay buffer in EGRL. While the PG learner fails to find full mapping solutions by itself, the partial solutions it finds carry vital information. The EA population in EGRL directly leverages this information to achieve better

mapping solutions than what it could find by itself. Greedy-DP outperforms the compiler, converging to 1.27 while PG converges to 0.23.

BERT: EGRL and EA significantly outperform the compiler as well as the other agents reaching a final speedup of 1.66 and 1.64, respectively. Greedy-DP converges to a speedup of 0.67, greatly underperforming the compiler. This is unsurprising as BERT is comparatively much larger in size than the two ResNet models. Thus, the simplistic assumption of conditional independence amongst node-level actions made by Greedy-DP begins to falter when the number of nodes increases. PG fails to find good mappings and converges to 0.21.

5.1 Generalization

Figure 5 reports the generalization performance of the GNN-policy used in EGRL after being trained on BERT and ResNet-50. Here, the GNN-policy is trained on one workload and performance is reported on other workloads without any fine-tuning. Results demonstrate that policies trained with either workload demonstrate

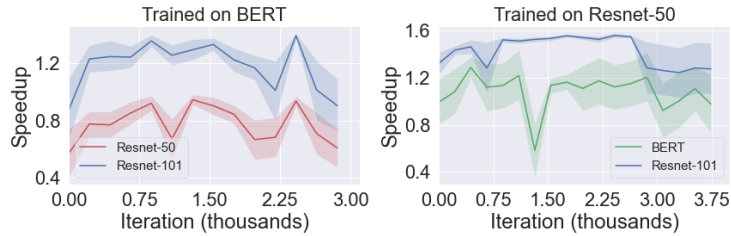


Figure 5: Zero-shot generalization: policies trained on one workload are tested on the others without fine-tuning

decent zero-shot transfer to other workloads. We observe some intermediate drops in transfer performance through training but the overall trend shows that the intermediate representation and knowledge encoded by the GNN policy transfers effectively to the other workloads. As training progresses, we see sharper dips and inconsistent transfer performance marked by larger variance. This is reminiscent of overfitting where the GNN-policy optimizes for the specifics of its training workload, degrading its ability to generalize.

5.2 Visualizing Memory Mappings

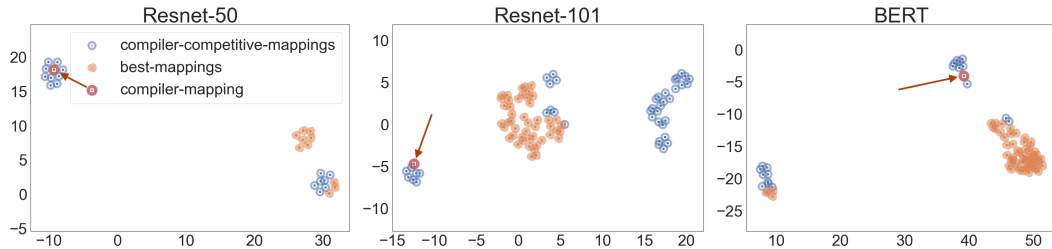


Figure 6: UMAP projection illustrating mappings that achieve compiler-competitive performance (speedup of ~ 1), the best mappings, and the compiler’s mapping (highlighted with a red arrow).

Fig 6 employs a UMAP embedding [McInnes et al., 2018] to illustrate the differences between the mapping solutions found by the compiler and during different phases of training. For each workload, we collected its mappings twice - first when the agent’s mappings approximately reach the compiler’s speedup performance (~ 1) denoted as **compiler-competitive-mappings**, and second when the agent reaches its best recorded speedup denoted as **best-mappings**. Since these mappings represent a collection of discrete decision per node, we represent them with a one-hot categorical expression and concatenate them across all nodes of the workload. Given this representation, we use the Jaccard distance [Niawattanakul et al., 2013] to compute the UMAP embedding. We also use a neighbour size of 8 to balance between the global and local structure captured by the projection.

Results show that compiler-competitive-mappings and best-mappings are well-separable across all three workloads. While we see some mixing, the general trend suggests strong separability between the two classes of mappings. Further, the compiler’s mapping also fell within the cluster of compiler-competitive-mappings across all three workloads. This suggests that the agents learn to mimic the

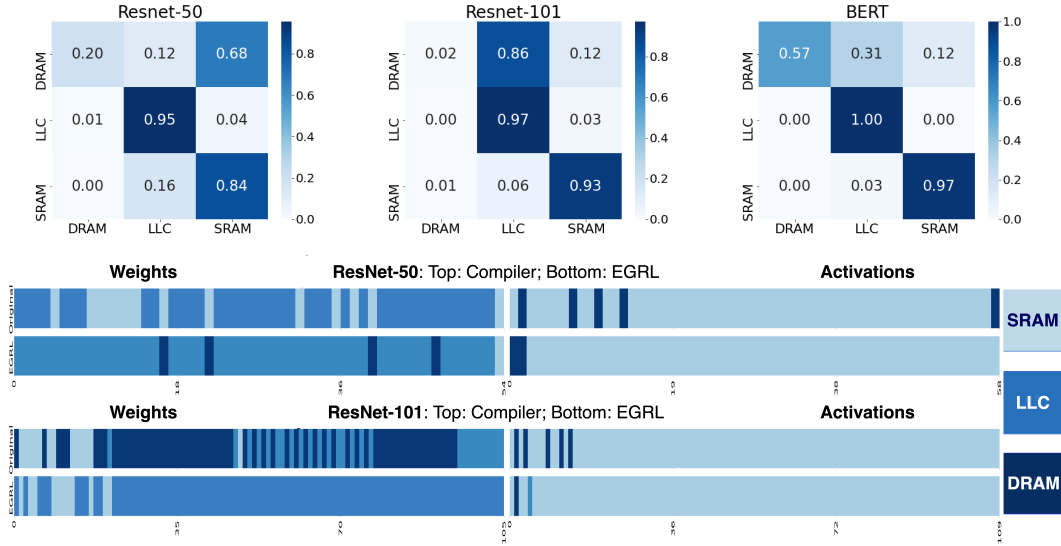


Figure 7: Memory map shifts **Top**: For each memory unit on the y-axis, the corresponding row shows how EGRL changed the distribution of tensors originally mapped to it by the compiler. **Bottom**: Memory maps from the compiler vs the best ones found by EGRL for ResNet-50 and ResNet-101. Each bar denotes a tensor operation.

compiler’s mappings at some point in their training. This is unsurprising as the reward we use to train the agents before they find valid mappings is based on differences with the compiler.

Interestingly, the intra-cluster spread for compiler-competitive-mappings is markedly higher than best-mappings across all three workloads. This indicates that the mappings associated with higher speedups are more self-similar than those that are less performant. This is unsurprising since the number of inferior mappings is higher than that of the superior ones.

5.2.1 Differences in Memory Mappings

Figure 7 provides some insights into the differences in mappings between the compiler and EGRL.

The transition matrices on top show a high-level view of how the distribution of tensors to the different memories shifted. Each row corresponds to a memory unit. The corresponding columns indicate how EGRL fractionally re-distributed tensors originally mapped to that unit into all available memories. At the bottom, we illustrate how each tensor in a workload was mapped by the compiler and by EGRL. Each band represents either a weight or an activation tensor.

While it is difficult to interpret the mapping decisions reliably, these visualizations indicate that EGRL generally found maps that avoided the slower but higher-capacity DRAM. This difference is particularly prominent for the weight tensors. EGRL also favored contiguity - where tensors from neighboring layers generally got mapped to the same type of memory. Both are performant strategies to optimize latency - but not trivial to achieve using heuristics that need to trade-off speed and capacity for a large number of tensors. EGRL’s graph-based global view of the workloads enables it to make globally optimal allocations compared to the sequential decision making of the compiler.

6 Discussion and Future Work

This paper introduced EGRL, a hybrid framework that pairs graph neural networks with population-based reinforcement learning to learn effective memory mapping solutions for large deep learning workloads. We train our policies end-to-end on the NNP-I chipset to ensure that the solutions are robust to the real-world constraints and uncertainties of the chip. Complimentary to other approaches like compression [Cheng et al., 2018, Kim et al., 2015], sparsification [Venkatesh et al., 2017] and network pruning [Han et al., 2015], EGRL keeps the workload unchanged and instead tackles how their tensors are mapped in hardware.

We show that EGRL scales effectively across varying sizes and operational types of DL workloads. Results show that EGRL outperforms several learning and search methods as well as the heuristic logic of the compiler. This scalability paves the way for learning-based agents to tackle other hardware mapping problems. Specifically, our future work will expand the action space of the EGRL agent to control other settings like batch size, ring frequencies, power efficiency and data decomposition.

7 Broader Impacts

We demonstrated the use of deep reinforcement learning in tackling the hardware mapping problem. Specifically, we showed that we can use GNN and population-based reinforcement learning to achieve a 28-78% speedup in inference on prominent deep learning models for computer vision (Resnet-50 and Resnet-101) and natural language processing (BERT). These models are key participants in the ongoing widespread proliferation of deep learning in industrial and consumer applications. For instance, ResNet-based models are frequently used in enabling autonomous driving [Chi and Mu, 2017, Teichmann et al., 2018] applications. Similarly, BERT is a key model used for real-world deployment of chatbots [Bathija et al., 2020], document understanding [Yang et al., 2019, Adhikari et al., 2019] and natural language processing [Tenney et al., 2019]. All these application are time-critical as they involve interaction with a customer. Further, some like autonomous driving are additionally safety-critical as a fast perception engine is crucial for effective and safe driving. The ability to maintain low latency is thus critical for both safety and scalability of such applications. The solution we develop in our paper is an enabling technology towards this goal.

One limitation of our solution is that the decisions taken by the RL agent are difficult to explain and understand. A broader shift towards RL based optimization, while improving overall performance, could therefore lead to lower explainability of the resulting solution. We are encouraged by the growing research in explainability related to deep learning algorithms and reinforcement learning to address this issue in a meaningful way.

As it pertains to using RL to automate design, one potential undesired effect is that by optimizing for greater throughput speeds, one might inadvertently over-optimize to a given metric without considering other important factors in the application. In the case of optimizing hardware, the RL agent may suggest a design that significantly decreases the lifetime of the hardware by overloading certain parts, which could also impact overall reliability of the hardware. Similarly, software products exposed to automatic agents need to be robustly designed so that the agent cannot manipulate the software to cause undesired side effects. One example is that the agent directly changes the compiler software or the firmware on the hardware itself which may cause undesired downstream effects. Moreover, if the decisions taken by RL agent are difficult to explain, this could lead to significant challenges in finding and resolving issues for a variety of applications, and lead to lower confidence in the applicability and reliability of many deep learning based methods.

References

- Martín Abadi, Paul Barham, Jianmin Chen, Zhifeng Chen, Andy Davis, Jeffrey Dean, Matthieu Devin, Sanjay Ghemawat, Geoffrey Irving, Michael Isard, et al. Tensorflow: A system for large-scale machine learning. In *12th {USENIX} Symposium on Operating Systems Design and Implementation ({OSDI} 16)*, pages 265–283, 2016.
- Ravichandra Addanki, Shaileshh Bojja Venkatakrishnan, Shreyan Gupta, Hongzi Mao, and Mohammad Alizadeh. Placeto: Efficient progressive device placement optimization. In *NIPS Machine Learning for Systems Workshop*, 2018.
- Ashutosh Adhikari, Achyudh Ram, Raphael Tang, and Jimmy Lin. Docbert: Bert for document classification. *arXiv preprint arXiv:1904.08398*, 2019.
- Rumen Andonov, Vincent Poirriez, and Sanjay Rajopadhye. Unbounded knapsack problem: Dynamic programming revisited. *European Journal of Operational Research*, 123(2):394–407, 2000.
- Kavosh Asadi and Michael L Littman. An alternative softmax operator for reinforcement learning. In *Proceedings of the 34th International Conference on Machine Learning-Volume 70*, pages 243–252. JMLR. org, 2017.

- Richeeka Bathija, Pranav Agarwal, Rakshith Somanna, and GB Pallavi. Guided interactive learning through chatbot using bi-directional encoder representations from transformers (bert). In *2020 2nd International Conference on Innovative Mechanisms for Industry Applications (ICIMIA)*, pages 82–87. IEEE, 2020.
- Richard Bellman. The theory of dynamic programming. *Bull. Amer. Math. Soc.*, 60(6):503–515, 11 1954. URL <https://projecteuclid.org:443/euclid.bams/1183519147>.
- Dimitris Bertsimas and Aurélie Thiele. A robust optimization approach to supply chain management. In *International Conference on Integer Programming and Combinatorial Optimization*, pages 86–100. Springer, 2004.
- Guy Boudoukh, Eli Kfir, Ofir Zafrir, Uzi Sarel, Michael Behar, Moshe Wasserblat, Galina Ryvchin, Peter Adams, and Kiran Atmakuri. Intel[®] Nervana[™] NNP-I shows best-in-class throughput on BERT NLP model. www.intel.com/content/www/us/en/artificial-intelligence/posts/nervana-nnp-i-shows-337best-in-class-throughput-on-bert-nlp-model.html, 2020.
- Tianqi Chen, Lianmin Zheng, Eddie Yan, Ziheng Jiang, Thierry Moreau, Luis Ceze, Carlos Guestrin, and Arvind Krishnamurthy. Learning to optimize tensor programs. In *Advances in Neural Information Processing Systems*, pages 3389–3400, 2018.
- Yu Cheng, Duo Wang, Pan Zhou, and Tao Zhang. Model compression and acceleration for deep neural networks: The principles, progress, and challenges. *IEEE Signal Processing Magazine*, 35(1):126–136, 2018.
- Lu Chi and Yadong Mu. Deep steering: Learning end-to-end driving model from spatial and temporal visual cues. *arXiv preprint arXiv:1708.03798*, 2017.
- Scott Cyphers, Arjun K Bansal, Anahita Bhiwandiwala, Jayaram Bobba, Matthew Brookhart, Avijit Chakraborty, Will Constable, Christian Convey, Leona Cook, Omar Kanawi, et al. Intel ngraph: An intermediate representation, compiler, and executor for deep learning. *arXiv preprint arXiv:1801.08058*, 2018.
- Hanjun Dai, Elias B. Khalil, Yuyu Zhang, Bistra Dilkina, and Le Song. Learning combinatorial optimization algorithms over graphs. *arXiv preprint arXiv:1704.01665*, 2018.
- Jeffrey Dean, Greg Corrado, Rajat Monga, Kai Chen, Matthieu Devin, Mark Mao, Marc’alelio Ranzato, Andrew Senior, Paul Tucker, Ke Yang, et al. Large scale distributed deep networks. In *Advances in neural information processing systems*, pages 1223–1231, 2012.
- Jacob Devlin, Ming-Wei Chang, Kenton Lee, and Kristina Toutanova. Bert: Pre-training of deep bidirectional transformers for language understanding. *arXiv preprint arXiv:1810.04805*, 2018.
- Dario Floreano, Peter Dürri, and Claudio Mattiussi. Neuroevolution: from architectures to learning. *Evolutionary Intelligence*, 1(1):47–62, 2008.
- David B Fogel. *Evolutionary computation: toward a new philosophy of machine intelligence*, volume 1. John Wiley & Sons, 2006.
- Scott Fujimoto, Herke van Hoof, and Dave Meger. Addressing function approximation error in actor-critic methods. *arXiv preprint arXiv:1802.09477*, 2018.
- Hongyang Gao and Shuiwang Ji. Graph u-nets. *arXiv preprint arXiv:1905.05178*, 2019.
- Marco Gori, Gabriele Monfardini, and Franco Scarselli. A new model for learning in graph domains. In *Proceedings. 2005 IEEE International Joint Conference on Neural Networks, 2005.*, volume 2, pages 729–734. IEEE, 2005.
- Tuomas Haarnoja, Aurick Zhou, Pieter Abbeel, and Sergey Levine. Soft actor-critic: Off-policy maximum entropy deep reinforcement learning with a stochastic actor. *arXiv preprint arXiv:1801.01290*, 2018.

- Song Han, Huizi Mao, and William J Dally. Deep compression: Compressing deep neural networks with pruning, trained quantization and Huffman coding. *arXiv preprint arXiv:1510.00149*, 2015.
- Kaiming He, Xiangyu Zhang, Shaoqing Ren, and Jian Sun. Deep residual learning for image recognition. In *Proceedings of the IEEE conference on computer vision and pattern recognition*, pages 770–778, 2016a.
- Kaiming He, Xiangyu Zhang, Shaoqing Ren, and Jian Sun. Deep residual learning for image recognition. In *Conference on Computer Vision and Pattern Recognition*, 2016b.
- Yihui He, Ji Lin, Zhijian Liu, Hanrui Wang, Li-Jia Li, and Song Han. Amc: Automl for model compression and acceleration on mobile devices. *arXiv preprint arXiv:1802.03494*, 2018.
- Norman P Jouppi, Cliff Young, Nishant Patil, David Patterson, Gaurav Agrawal, Raminder Bajwa, Sarah Bates, Suresh Bhatia, Nan Boden, Al Borchers, et al. In-datacenter performance analysis of a tensor processing unit. In *Proceedings of the 44th Annual International Symposium on Computer Architecture*, pages 1–12, 2017.
- Shauharda Khadka and Kagan Tumer. Evolution-guided policy gradient in reinforcement learning. In *Advances in Neural Information Processing Systems*, pages 1196–1208, 2018.
- Shauharda Khadka, Somdeb Majumdar, Tarek Nassar, Zach Dwiell, Evren Tumer, Santiago Miret, Yinyin Liu, and Kagan Tumer. Collaborative evolutionary reinforcement learning. *arXiv preprint arXiv:1905.00976v2*, 2019.
- Yong-Deok Kim, Eunhyeok Park, Sungjoo Yoo, Taelim Choi, Lu Yang, and Dongjun Shin. Compression of deep convolutional neural networks for fast and low power mobile applications. *arXiv preprint arXiv:1511.06530*, 2015.
- Benno Lüders, Mikkel Schläger, Aleksandra Korach, and Sebastian Risi. Continual and one-shot learning through neural networks with dynamic external memory. In *European Conference on the Applications of Evolutionary Computation*, pages 886–901. Springer, 2017.
- Peter Mattson, Vijay Janapa Reddi, Christine Cheng, Cody Coleman, Greg Diamos, David Kanter, Paulius Micikevicius, David Patterson, Guenther Schmuelling, Hanlin Tang, et al. Mlperf: An industry standard benchmark suite for machine learning performance. *IEEE Micro*, 40(2):8–16, 2020.
- Leland McInnes, John Healy, Nathaniel Saul, and Lukas Großberger. Umap: Uniform manifold approximation and projection. *Journal of Open Source Software*, 3(29), 2018.
- Azalia Mirhoseini, Anna Goldie, Mustafa Yazgan, Joe Jiang, Ebrahim Songhori, Shen Wang, Young-Joon Lee, Eric Johnson, Omkar Pathak, Sungmin Bae, Azade Nazi, Jiwoo Pak, Andy Tong, Kavya Srinivasa, William Hang, Emre Tuncer, Anand Babu, Quoc V. Le, James Laudon, Richard Ho, Roger Carpenter, and Jeff Dean. Chip placement with deep reinforcement learning. *arXiv preprint arXiv:2004.10746*, 2020.
- Akash Mittal, Anuj Dhawan, Sahil Manchanda, Sourav Medya, Sayan Ranu, and Ambuj Singh. Learning heuristics over large graphs via deep reinforcement learning. *arXiv preprint arXiv:1903.03332*, 2019.
- Suphakit Niwattanakul, Jatsada Singthongchai, Ekkachai Naenudorn, and Supachanun Wanapu. Using of jaccard coefficient for keywords similarity. In *Proceedings of the international multiconference of engineers and computer scientists*, volume 1, pages 380–384, 2013.
- Aditya Paliwal, Felix Gimeno, Vinod Nair, Yujia Li, Miles Lubin, Pushmeet Kohli, and Oriol Vinyals. Reinforced genetic algorithm learning for optimizing computation graphs. *arXiv preprint arXiv:1905.02494*, 2020.
- Jongsoo Park, Maxim Naumov, Protonu Basu, Summer Deng, Aravind Kalaiah, Daya Khudia, James Law, Parth Malani, Andrey Malevich, Satish Nadathur, et al. Deep learning inference in facebook data centers: Characterization, performance optimizations and hardware implications. *arXiv preprint arXiv:1811.09886*, 2018.

- Adam Paszke, Sam Gross, Soumith Chintala, Gregory Chanan, Edward Yang, Zachary DeVito, Zeming Lin, Alban Desmaison, Luca Antiga, and Adam Lerer. Automatic differentiation in pytorch. In *Advances in Neural Information Processing Systems*, 2018.
- Vijay Janapa Reddi, Christine Cheng, David Kanter, Peter Mattson, Guenther Schmuelling, Carole-Jean Wu, Brian Anderson, Maximilien Breughe, Mark Charlebois, William Chou, et al. Mlperf inference benchmark. *arXiv preprint arXiv:1911.02549*, 2019.
- Franco Scarselli, Marco Gori, Ah Chung Tsoi, Markus Hagenbuchner, and Gabriele Monfardini. The graph neural network model. *IEEE Transactions on Neural Networks*, 20(1):61–80, 2008.
- Zhan Shi, Xiangru Huang, Akanksha Jain, and Calvin Lin. Applying deep learning to the cache replacement problem. In *Proceedings of the 52nd Annual IEEE/ACM International Symposium on Microarchitecture*, pages 413–425, 2019.
- William M Spears, Kenneth A De Jong, Thomas Bäck, David B Fogel, and Hugo De Garis. An overview of evolutionary computation. In *European Conference on Machine Learning*, pages 442–459. Springer, 1993.
- Sainbayar Sukhbaatar, Rob Fergus, et al. Learning multiagent communication with backpropagation. In *Advances in neural information processing systems*, pages 2244–2252, 2016.
- Marvin Teichmann, Michael Weber, Marius Zoellner, Roberto Cipolla, and Raquel Urtasun. Multinet: Real-time joint semantic reasoning for autonomous driving. In *2018 IEEE Intelligent Vehicles Symposium (IV)*, pages 1013–1020. IEEE, 2018.
- Ian Tenney, Dipanjan Das, and Ellie Pavlick. Bert rediscovers the classical nlp pipeline. *arXiv preprint arXiv:1905.05950*, 2019.
- Ganesh Venkatesh, Eriko Nurvitadhi, and Debbie Marr. Accelerating deep convolutional networks using low-precision and sparsity. In *2017 IEEE International Conference on Acoustics, Speech and Signal Processing (ICASSP)*, pages 2861–2865. IEEE, 2017.
- Chao Wang, Lei Gong, Qi Yu, Xi Li, Yuan Xie, and Xuehai Zhou. Dlau: A scalable deep learning accelerator unit on fpga. *IEEE Transactions on Computer-Aided Design of Integrated Circuits and Systems*, 36(3):513–517, 2016.
- Kuan Wang, Zhijian Liu, Yujun Lin, Ji Lin, and Song Han. Haq: Hardware-aware automated quantization with mixed precision. *CVPR*, 2019.
- O. Wechsler, M. Behar, and B. Daga. Spring hill (nnp-i 1000) intel’s data center inference chip. In *2019 IEEE Hot Chips 31 Symposium (HCS)*, pages 1–12. IEEE, 2019.
- Zonghan Wu, Shirui Pan, Fengwen Chen, Guodong Long, Chengqi Zhang, and S Yu Philip. A comprehensive survey on graph neural networks. *IEEE Transactions on Neural Networks and Learning Systems*, 2020.
- Bing Xu, Naiyan Wang, Tianqi Chen, and Mu Li. Empirical evaluation of rectified activations in convolutional network. *arXiv preprint arXiv:1505.00853*, 2015.
- Wei Yang, Haotian Zhang, and Jimmy Lin. Simple applications of bert for ad hoc document retrieval. *arXiv preprint arXiv:1903.10972*, 2019.
- Rex Ying, Ruining He, Kaifeng Chen, Pong Eksombatchai, William L Hamilton, and Jure Leskovec. Graph convolutional neural networks for web-scale recommender systems. In *Proceedings of the 24th ACM SIGKDD International Conference on Knowledge Discovery & Data Mining*, pages 974–983, 2018.
- Lei Zhang, Reza Karimi, Irfan Ahmad, and Ymir Vigfusson. Optimal data placement for heterogeneous cache, memory, and storage systems. *Proceedings of the ACM on Measurement and Analysis of Computing Systems*, 2020.
- Brian D Ziebart, Andrew L Maas, J Andrew Bagnell, and Anind K Dey. Maximum entropy inverse reinforcement learning. In *AAAI*, volume 8, pages 1433–1438. Chicago, IL, USA, 2008.

A Graph Embedding

Table 1 details the features we used for the node embedding. These features encapsulate information about the input and output tensors of the given operation, as well as summary information about future layers.

Node Features	Description
<i>op_id</i>	Operation id
<i>weight_size</i>	Size in bytes of the weights if exist, 0 otherwise
<i>ifm_x</i>	Input feature map size on the x axis
<i>ifm_y</i>	Input feature map size on the y axis
<i>ifm_z</i>	Input feature map size on the z axis
<i>ofm_x</i>	Output feature map size on the x axis
<i>ofm_y</i>	Output feature map size on the y axis
<i>ofm_z</i>	Output feature map size on the z axis
<i>ifm_size</i>	Total size of the input feature map ($ifm_x * ifm_y * ifm_z$)
<i>ofm_size</i>	Total size of the onput feature map ($ofm_x * ofm_y * ofm_z$)
<i>n_ops_left</i>	Total number of operations after current <i>node</i>
<i>n_w_left</i>	Total number of weights from current <i>node</i> to the last node
<i>groups</i>	Number of groups - Convolution related parameter, set to 0 otherwise
<i>kernel_x</i>	Kernel size on x axis - Convolution related parameter, set to 0 otherwise
<i>kernel_y</i>	Kernel size on y axis - Convolution related parameter, set to 0 otherwise
<i>stride</i>	Stride size - Convolution related parameter, set to 0 otherwise
<i>pad</i>	Padding size - Convolution related parameter, set to 0 otherwise
<i>dilation</i>	Dilation - Convolution related parameter, set to 0 otherwise
<i>batch</i>	Input batch size

Table 1: GNN Node Features

B Hyperparameters

Table 2 details the hyperparameters used in the paper.

Hyperparameter	Range explored	Value used
GNN hidden layer size	[32, 64, 128]	128
GNN output layer size	[32, 64, 128]	128
GNN depth	4	4
Number of GNN attention heads	[1, 4]	4
# Steps per Episode	[1, 5, 10]	1
Initial mapping action	['DRAM']	'DRAM'
Reward for invalid mapping	[-10, -1]	-1
Discount Rate	[0.9, 0.97, 0.99]	0.99
EA population size	[10, 20]	20
PG Rollout size	[0, 1, 10]	1
Fraction of EA population that are Boltzmann	[0.1, 0.2, 0.5]	0.2
Total steps in the environment	[4000, 10000]	4000
Replay buffer size	[100000]	100000
Critic learning rate	[1e-3, 1e-4]	1e-3
Actor learning rate	[1e-3, 1e-4]	1e-3
Alpha (Entropy Coefficient)	[0.05, 0.1, 0.2]	0.05
Tau (Double-Q Network synchronization rate)	[1e-3]	1e-3
Batch size for PG	24	24
Reward scaling multiplier	5	5
Gradients steps per environment step	1	1

Table 2: Hyperparameters

C EGRL

Algorithm 2 EGRL Algorithm

```

1: Initialize a mixed population of  $k$  policies  $pop_\pi$ 
2: Initialize an empty cyclic replay buffer  $\mathcal{R}$ 
3: Define a random number generator  $r() \in [0, 1)$ 
4: for generation = 1,  $\infty$  do
5:   for actor  $\pi \in pop_\pi$  do
6:     fitness, Experiences = Rollout( $\pi$ )
7:     Add experiences to  $\mathcal{R}$ 
8:   end for
9:   Rank the population based on fitness scores
10:  Select the first  $e$  actors  $\pi \in pop_\pi$  as elites
11:  Select  $(k - e)$  actors  $\pi$  from  $pop_\pi$ , to form Set  $S$  using tournament selection with replacement
12:  while  $|S| < (k - e)$  do
13:    Select  $\pi_a \in e$  and  $\pi_b \in S$ 
14:    if  $\pi_a$  and  $\pi_b$  are of the same encoding type then
15:      Use single-point crossover and append to  $S$ 
16:    else
17:      Sample a random state and get action  $a$  from the GNN policy
18:      Use  $a$  to encode the prior of the Boltzmann chromosome
19:    end if
20:  end while
21:  for Actor  $\pi \in Set S$  do
22:    if  $r() < mut_{prob}$  then
23:      Mutate( $\theta^\pi$ ) by adding noise  $\sim \mathcal{N}(0, \sigma)$ 
24:    end if
25:  end for
26:  ups = # of environment steps taken this generation
27:  for ii = 1, ups do
28:    Sample a random minibatch of T transitions  $(s_i, a_i, r_i, s_{i+1})$  from  $\mathcal{R}$ 
29:    Update the critic via a Bellman update
30:     $L_i = \frac{1}{T} \sum_i (y_i - Q_i(s_i, a_i^\sim))^2$ 
31:    where  $y_i = r_i + \gamma \min_{j=1,2} Q'_j(s_{i+1}, a_{i+1}) + H(\pi(\cdot | s_{i+1}))$ 
32:    where  $a_i^\sim = a_i + \epsilon, clip(\epsilon \sim \mathcal{N}(\mu, \sigma^2) - c, c)$ 
33:    Update  $L_\pi$  using the sampled policy gradient with noisy actions
34:    Soft update target networks:
35:     $L_{\theta^{\pi'}} \leftarrow \tau L_{\theta^\pi} + (1 - \tau) L_{\theta^{\pi'}}$  and
36:     $L_{\theta^{\varnothing'}} \leftarrow \tau L_{\theta^\varnothing} + (1 - \tau) L_{\theta^{\varnothing'}}$ 
37:  end for
38:  Copy  $L_\pi$  into the population: for weakest  $\pi \in pop_\pi : \theta^\pi \leftarrow L_{\theta^\pi}$ 
39: end for

```

EGRL incorporates EA’s population-based search with powerful gradient-based methods from DRL to expedite learning. In this work, we instantiate the EA population to use both the GNN encodings as well as a Boltzmann chromosome encoding to direct its search. Concurrently, we use a modified SAC Haarnoja et al. [2018] algorithm as our gradient-based technique in training the GNN policies. Algorithm 2 details the EGRL algorithm.

A general flow of the EGRL algorithm proceeds as follow: a mixed population of GNN-policies and Boltzmann-based policies is initialized with random weights. In addition to the population, one additional actor network (referred to as pg_{gnn} henceforth) is initialized alongside a critic network. The population is then evaluated in the environment by allowing it to control the memory mapping for the specified workload in SPH hardware. A selection operator then selects a portion of the population for survival with probability commensurate on their relative performance. The population is then probabilistically *perturbed* through mutation and crossover operations to create the next generation. A select portion top performers are preserved as elites and are shielded from the mutation step.

Shared Replay Buffer: Unlike a traditional evolutionary population, each individual (whether GNN or Boltzmann-based) stores its experience defined by the tuple (*current state, action, next state, reward*) in a globally shared replay buffer. This is done for every interaction that takes place with the hardware to maximize data efficiency. The critic samples a random minibatch from this shared replay buffer and uses it to update its parameters using gradient descent. The critic is then used to train the pg_{gnn} using the sampled policy gradient.

The shared replay buffer is a key mechanism that enables the sharing of information across the varying learning methods. In contrast to a standard search method which would extract the performance score and disregard the underlying data immediately, EGRL retains every interaction in the global buffer and engages the pg_{gnn} and critic to learn from them repeatedly using powerful gradient-based methods. This enables maximal information extraction from each individual experiences as interfacing with the hardware is an expensive operation.

Mixed Exploration: A noisy version of the pg_{gnn} using Gaussian noise generator is used to generate additional experiences for the replay buffer. In contrast to the population of GNN-actors which explore by noise in their neural weights, the pg_{gnn} actors explore through noise in its *action space*. Boltzmann chromosomes tread this line in between where they explore in the parameters space more directly connected to the action space. Overall, each exploration technique are complementary and collectively lead to an effective exploration of the solution space.

Migration: Periodically, the pg_{gnn} network’s weights are copied into the evolutionary population. This process enables the evolutionary framework to directly leverage the information learned through gradient descent. This process also serves to stabilize learning and make it more robust to deception. If the policy learned by the pg_{gnn} is favorable, it will be selected to survive and extend its influence to the population over subsequent generations. However, in case it is bad, it will be selected against and discarded. This mechanism ensures that the flow of information from the pg_{gnn} to the evolutionary population is constructive.

D Policy Gradient modifications to SAC

Policy Gradient Algorithm: We build on SAC [Haarnoja et al., 2018] to tackle our large multi-discrete actions space. Since our policy is discrete, we compute entropy directly as

$$H(\pi(\cdot|s)) = \mathbb{E}_{s \sim D} \left[- \sum \pi(\cdot|s) \log \pi(\cdot|s) \right]$$

We then average over all nodes to compute the overall entropy of the policy. Further, we use a noisy version of the one-hot encoded behavioral action to compute our Bellman update as

$$L_i = \frac{1}{T} \sum_i (y_i - Q_i(s_i, \tilde{a}_i))^2$$

where $y_i = r_i + \gamma \min_{j=1,2} Q'_j(s_{i+1}, a_{i+1}) + H(\pi(\cdot|s_{i+1}))$

We use the minimum of two heads from the Q-Network based on [Fujimoto et al., 2018]. The noisy action \tilde{a}_i is computed by adding Gaussian noise clipped between $-c$ and c

$$\tilde{a}_i = a_i + clip(\epsilon \sim \mathcal{N}(\mu, \sigma^2), -c, c)$$

This noisy action smoothens the value estimate towards similar state-action value estimates by the policy. It serves to make the policy smooth and addresses overfitting to the one-hot encoded behavioral output. The actor is trained using the sampled policy gradient.

E Boltzmann Chromosome

Figure 8 illustrates the operation of the Boltzmann chromosome for a particular action choice in one node. Parameters for prior (p_1, p_2, p_3) and temperature t fully encode the chromosome’s policy. To compute an action, we first compute the probabilities by applying the Boltzmann softmax operation with the associated prior and temperature. Action is the sampled from this probability distribution. The choice of temperature t directly modulates the exploration-exploitation knob of decision making. A higher temperature leads to higher entropy probability distribution enabling higher exploration. In contrast, a lower value of temperature will lead to lower entropy in the probability distribution enabling exploitation of the prior information.

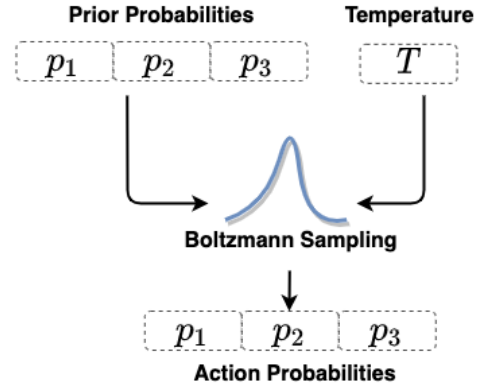


Figure 8: Boltzmann Chromosome for a node

For the agent policy described in this paper, a Boltzmann chromosome solution comprises of priors and temperature parameters for each node and action choice in the computational graph. Learning either through seeding, mutation or crossover involves a direct update of these parameters. Importantly, these parameters are learned independently within the context of each node allowing for varying degrees of exploration-exploitation position across nodes. For instance, the agent could be very confident about mapping a specific node while concurrently be unsure for a different node of the same workload at the same time. This enables the agent to systematically balance the exploration-exploitation tradeoff at the resolution of individual node actions.